Synthesis and Electrochemical Properties of Spinel LiCrTiO$_4$ and Its Application in LiFePO$_4$/LiCrTiO$_4$ Full Cells

Hualing Tian, Zhi Su[*], Yanhui Zhang

College of Chemistry and Chemical Engineering , Xinjiang Normal University,Urumqi, 830054, Xinjiang, China
[*]E-mail: suzhixj@sina.com

Spinel structure LiCrTiO$_4$ was prepared through a solid-state reaction using Li$_2$CO$_3$, Cr$_2$O$_3$, and TiO$_2$ as raw materials. X-ray diffraction (XRD), X-ray photoelectron spectroscopy (XPS), transmission electron microscopy (TEM), scanning electron microscopy (SEM) was used to characterize the structure of LiCrTiO$_4$. Electrochemical properties of LiCrTiO$_4$ were studied by cyclic voltammetry (CV), electrochemical impedance spectroscopy (EIS) and charge-discharge cycling performance. Electrochemical testing showed that LiCrTiO$_4$ has an excellent electrochemical capacity of 164 mAh·g^{-1} at a 0.5C-rate, and 116.1mAh·g^{-1} at a 10C-rate with stable cycling performance. Furthermore, LiFePO$_4$/LiCrTiO$_4$ full cells were constructed using LiCrTiO$_4$ as the anode electrode that displayed superior cycling stability at high rates. The LiFePO$_4$/LiCrTiO$_4$ full cell exhibited a charge capacity of 136.6mAh·g^{-1} and discharge capacity of 116mAh·g^{-1} at a 0.2C-rate, and 96.4mAh·g^{-1} at 2C-rate.

1. INTRODUCTION

Lithium-ion batteries have become the primary choice for green batteries in the 21st century because of their high energy density, low cost, no memory and high-rate capability. Graphite is used as the anode material in commercial lithium-ion batteries. Graphite anode materials have a high specific capacity of 372mAh·g^{-1}, but a poor rate performance and serious security problems[1,2]. Therefore, graphite cannot satisfy the requirements of portable electronic devices. Much effort has been invested in the exploration of new lithium-ion battery anode materials to meet the demands for a long cycle life and environmental friendliness. Spinel Li$_4$Ti$_5$O$_{12}$ has attracted considerable attention because it has a higher Li-insertion voltage (ca.1.5Vvs.Li/Li$^+$) and in addition, it is a zero-strain insertion material[3-5]. However, Li$_4$Ti$_5$O$_{12}$ shows an inadequate rate performance because of its low electrical conductivity

and poor Li-ion diffusion properties[6,7]. Therefore, the aforementioned advantages of $Li_4Ti_5O_{12}$ have stirred up a continuous interest for many researchers though the energy density of LIBs is slightly sacrificed when it is coupled with a 4V cathode material. However $Li_4Ti_5O_{12}$ usually show poor high rate performance because of its poor electronic conductivity and poor Li-ion diffusion properties. Thus, finding an anode material with good cycle stability and rate performance is important. Spinel $LiCrTiO_4$ exhibits flat discharge potential curves at ~1.5Vvs.Li^+/Li and a theoretical capacity of 157mAh·g^{-1}, similar to its $Li_4Ti_5O_{12}$ counterpart[8-10]. Studies show that Li/$LiCrTiO_4$ half-cells have a long cycle life, high coulombic efficiency, and an excellent rate performance. In addition, olivine-structured $LiFePO_4$ is considered a promising cathode material, due to its stable framework, low cost, low toxicity, a moderate flat potential of 3.45Vvs.Li^+/Li and a theoretical capacity of 170mAh·g^{-1}[11-13]. Currently, $LiFePO_4$ is being widely used in electronic products. Hence, a combination of $LiCrTiO_4$ and $LiFePO_4$ may create a much-improved Li-ion battery system.

The paper report that the synthesis of the $LiCrTiO_4$ materials by using a solid-state reaction method and the $LiFePO_4$/C composite materials by using carbothermal reduction technology method. Meanwhile, the electrochemical performance of $LiFePO_4$/$LiCrTiO_4$ full cells were investigated in particular detail.

2. EXPERIMENTAL

2.1 Preparation of LiCrTiO4 and LiFePO4/C

$LiCrTiO_4$ materials was synthesized via a solid-state reaction. A stoichiometric amount of TiO_2 (AR ≥99.0%), Li_2CO_3 (AR ≥98.0%) (2.5% mass excess), and Cr_2O_3 (AR ≥99.0%) (Li:Cr:Ti = 1.1:1:1) were manually mixed using a mortar and pestle and then sintered at 800°C for 12h in a tubular furnace in air and afterwards quenched to room temperature. This procedure resulted in particulate $LiCrTiO_4$.

$LiFePO_4$/C cathode materials were prepared via a carthothermal method. Stoichiometric quantities of LiH_2PO_4, Fe_2O_3 and glucose (ca.20wt%) were mixed together using a planet mixer for 4 h in ethyl alcohol. After milling, the mixture was dried at 60°C for 8h in a blast oven. The dried powder was then transferred to a ceramic boat. Later, the ceramic boat was thermally treated under an N_2 flow at 700°C for 12h. After treatment, olivine-structured $LiFePO_4$/C was successfully generated.

2.2 Characterization

The identification of the $LiCrTiO_4$($LiFePO_4$/C) phase was conducted using powder X-ray diffraction (XRD, Bruker D2) with Cu K-a radiation. The diffraction data were collected using the step mode over an angular range of 10–70°, with a step size of 0.02° at 30kV and 10mA. Scanning electron microscopy (SEM,Germany Zeissm Supra 55VP) images were collected at 20kV. The transmission electron microscopy (TEM, Philips CM10) images of the samples were collected at an accelerating voltage of 200kV.

The electrochemical performance of the samples was assessed using coin-type half cells (LIR 2025) that were assembled in an argon glove box. The anode was fabricated by mixing 80wt% active material, 15wt% acetylene black and 5wt% polytetrafluoroethylene (PTFE) in deionized water. The obtained slurry was coated on an Cu foil and dried at 80°C for 12h under vacuum. The electrolyte consisted of 1M $LiPF_6$ in a mixture of ethylene carbonate/dimethyl carbonate (EC/DMC) (1: 1 by volume). The cathode materials was fabricated by mixing 80wt% active material, 15wt% acetylene black and 5wt% polytetrafluoroethylene (PTFE) in deionized water. The obtained slurry was coated on an Cu foil and dried at 80°C for 12h under vacuum. The electrolyte consisted of 1M $LiPF_6$ in a mixture of ethylene carbonate/dimethyl carbonate (EC/DMC) (1 :1 by volume).

The LAND CT2001A galvanostatic method was used to measure the electrochemical capacity and cycle performance of the electrodes at room temperature. The charge and discharge profiles of the $LiCrTiO_4$ cut-off potentials were set to 1.0 and 3.0V, The $LiFePO_4$/C at a voltage ranging between 2.5 and 4.3V and the $LiFePO_4$/$LiCrTiO_4$ full cell were tested between 0.5 and 2.5V and measured at variable current densities. Cyclic voltammetry (CV, LK2500) was performed from 1.0 to 3.0V (2.5~4.3V) with a scan rate of $0.1mV·s^{-1}$. Electrochemical impedance spectroscopy (EIS, Zahner IM6ex) was completed over a frequency range of 10kHz to 10mHz, with a 5mVa.c. input signal applied between the working and reference electrodes.

3. RESULTS AND DISCUSSION

3.1 Composition and structure characterization

XRD patterns of $LiCrTiO_4$ and $LiFePO_4$/C are shown in Fig.1. Fig.1(a) shows the formation of $LiCrTiO_4$ particles synthesized by the solid-state reaction method. The sharp diffraction peaks indicate good crystallinity of the samples. The powder XRD pattern shows well-defined crystalline peaks without any traces of impurity, which is similar to XRD patterns previously published. Which is also in good agreement with the data reported in the literature (JCPDS 47-0139,α=8.313(2)Å). In addition, all of the XRD patterns show the materials to be highly ordered, indicating that a product with high purity was synthesized[10,14]. The as-prepared $LiFePO_4$/C composite is shown in Fig.1(b). All peaks can be indexed as a pure and well-crystallized $LiFePO_4$ phase with an olivine structure and a space group of Pnma (JCPDS 83-2092). Nearly all diffraction peaks of LiH_2PO_4 and Fe_2O_3 vanished with the appearance of the diffraction peaks for $LiFePO_4$, which is also similar to previous literature reports.

TEM and HRTEM images of the $LiFePO_4$/C are shown in Fig.2a, respectively. Fig.2a shows that $LiFePO_4$/C consists of relatively larger particles with a grain diameter in the range of 30-150nm. The HRTEM images of $LiFePO_4$/C, it can be seen from Fig.2a that $LiFePO_4$/C exhibits regular lattice fringes of the (022) crystalline plane with a measured d-spacing value of 0.33nm. And the amorphous carbon layers just coat over the surfaces of these large particles of $LiFePO_4$/C coating layer has no influence on the crystal state of original cathode materials[10-12].
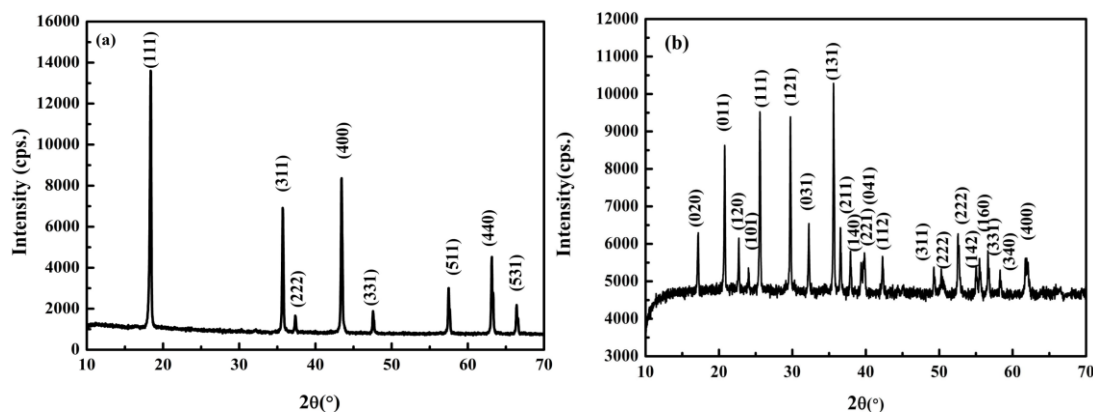
Figure 1. (a) XRD pattern of LiCrTiO$_4$, and (b) XRD pattern of LiFePO$_4$/C.

Fig.2b shows the SEM images of the as-prepared samples of LiCrTiO$_4$. It's thus clear that the blocky-shaped large particles of LiCrTiO$_4$ have been observed in SEM measurement and they are formed from the close packing of small crystal grains with the size ranged from several nanometers to over 300 nanometers[13-15].
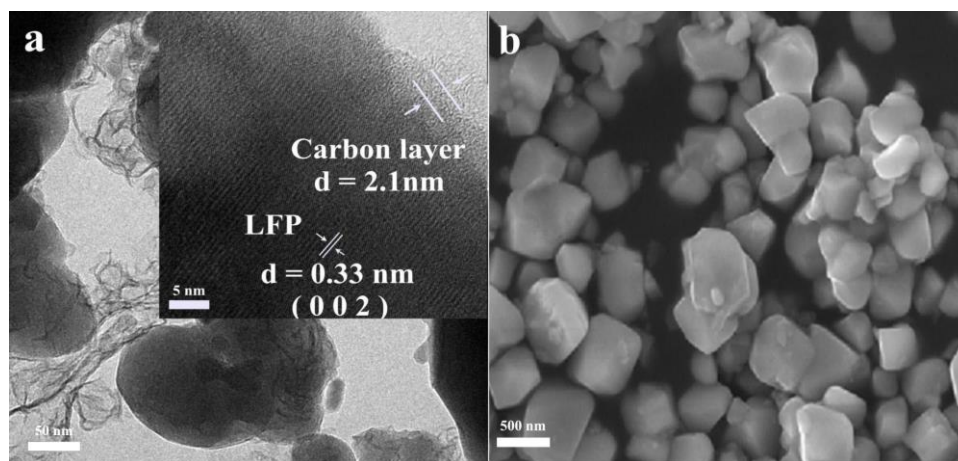

Figure 2. TEM and HRTEM images of (a) LiFePO$_4$/C, SEM images of (b) LiCrTiO$_4$.

The valence states of Fe and P in the LiFePO$_4$/C composite were obtained through XPS. In Fig. 3a, the XPS spectra of P2p showed that with binding energies of 133.58eV, which can be assigned to P2p. The binding energies of the peak matched well with that observed in LiFePO$_4$, indicating that the oxidation states of phosphorus is+5[16-18]. It can be found from Fig.3b that the XPS spectrum of Fe2p can be split into two spectra Fe2p1/2 and Fe2p3/2 with binding energies of 726.58eV and 710.98 eV. The result shows that the valence of Fe in the composite is +2[19,20]. It can be seen from Fig.3c the XPS spectra of Cr2p shows that with binding energies of 576.6eV, 578eV and 585eV. which correspond to Cr2p3/2, Cr2p3/2 and Cr2p1/2 core-level binding energies of Cr^{3+}, respectively[21]. The LiCrTiO$_4$ samples showed two peaks at 458 and 464eV(Fig.3d), which correspond to Ti2p3/2 and Ti2p1/2 core-level binding energies of Ti^{4+}[22-23], respectively.
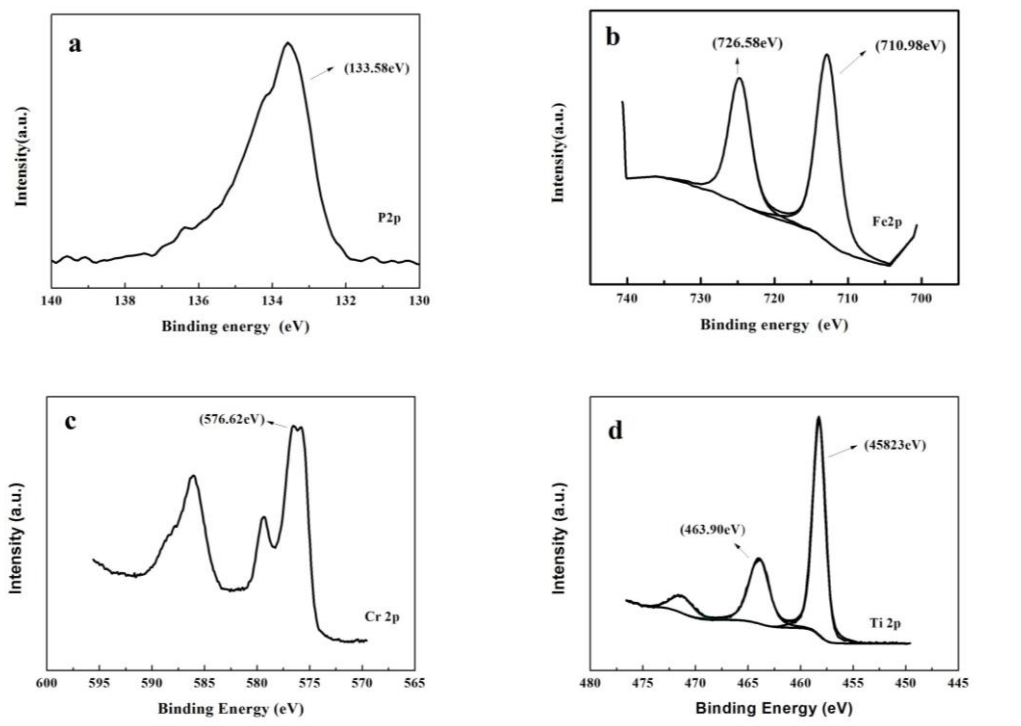
Figure 3. XPS spectra of P2p (a) and Fe2p (b) in LiFePO$_4$/C and XPS spectra of Cr2p(c) and Ti2p (d) in LiCrTiO$_4$.

3.2 Electrochemical performance of LiCrTiO$_4$ and LiFePO$_4$/C

Charge/discharge curves of as-synthesized LiCrTiO$_4$ powders sintered at 800°C for 12h at current densities ranging from 0.5C to 10C in the voltage range of 1.0-3.0V are shown in Fig.4(a). All samples exhibit three pairs of visible and flat plateaus of charge 1.6V and discharge of 1.5V[17,18] that indicate the characteristics of the electrochemical reaction producing LiCrTiO$_4$ from Li$_2$CrTiO$_4$. The galvanostatic rate performances of LiCrTiO$_4$ are shown in Fig.4(b). The half-cell displayed a capacity of 164mAh·g^{-1} and 162mAh·g^{-1} at a current density of 0.5C for the initial discharge and charge, respectively. The initial discharge capacity is slightly higher than the theoretical capacity (157mAh·g^{-1})[23], because the structural change and solid electrolyte interphase (SEI) formation of the electrode were completed in five cycles. Five cycles later, the discharge capacity leveled at 155 mAh·g^{-1}. The capacities of LiCrTiO$_4$ at 0.5, 1, 2, 5 and 10C were 155, 150, 143, 130 and 116mAh·g^{-1}, respectively. The coulombic efficiency at different current densities remained at~100%, showing an excellent reversible Li$^+$ insertion/extraction process and better rate performance. Fig.4(c) shows the discharge curves for LiFePO$_4$/C at a charge-discharge rate of 0.2C, which show potential plateaus at 3.4V and 3.3V versus Li/Li$^+$[24-26]. All of these samples demonstrated excellent cycling stability, with hardly any decrease after 50cycles. LiFePO$_4$/C retained 97.8% (156.6mAh·g^{-1}) of the initial specific discharge capacity after 50cycles, demonstrating excellent cycling performance.
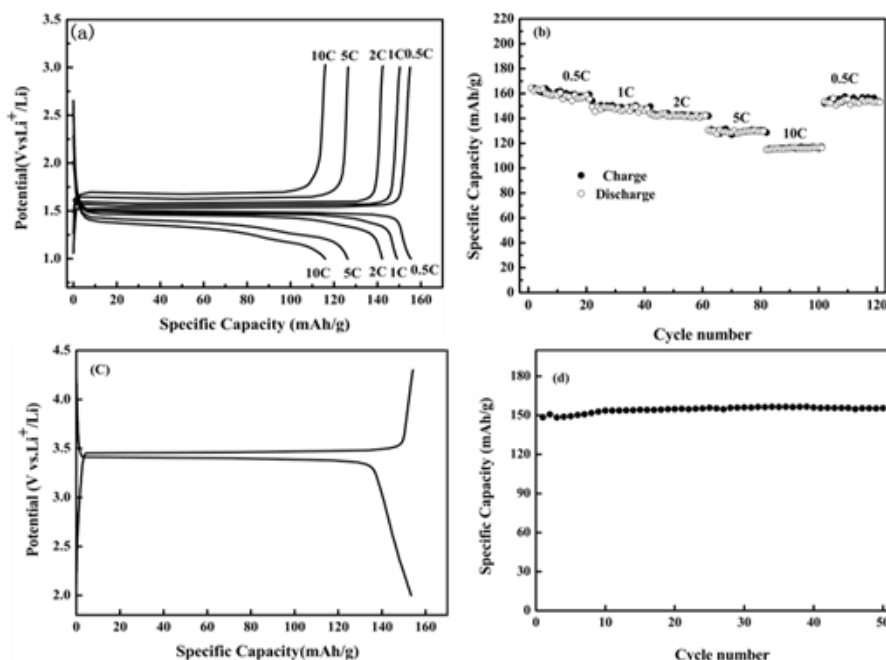
Figure 4. (a) Charge and discharge curves of $LiCrTiO_4$ samples at 0.5C, 1C, 2C, 5C and 10C, (b) cycling performance of $LiCrTiO_4$ at 0.5C, 1C, 2C, 5C and 10C in the voltage range of 1.0-3.0 V, (c) charge and discharge curves of $LiFePO_4/C$ at 0.2C, (d) cycling performance of $LiFePO_4/C$ at 0.2C in the voltage range of 2.0-4.3V.

3.3 Electrochemical performance of $LiCrTiO_4/ LiFePO_4$

$LiCrTiO_4$ served as the anode material and $LiFePO_4$ served as the cathode material, which together produced a $LiFePO_4/LiCrTiO_4$ full cell. In this particular full cell, the anode electrode whose materials were in slight excess, so the specific capacity of the battery was calculated via the active cathode material. Charge and discharge curves for this $LiFePO_4/LiCrTiO_4$ full cell are shown in Fig. 5(a). The charge-discharge performances were measured at 0.2, 0.5, 1 and 2C in the voltage range of 0.5-2.4V at room temperature. Flat plateaus were observed at 1.85V[27,28]. This $LiFePO_4/LiCrTiO_4$ full cell sample exhibited a charge capacity of 136.6mAh·g^{-1} and discharge capacity of 116mAh·g^{-1} at 0.2C.

The cycle performance of the $LiFePO_4/LiCrTiO_4$ full cell was tested at different current densities corresponding to 0.2, 0.5, 1 and 2C. The $LiFePO_4/LiCrTiO_4$ full cell sample in this study showed a good rate capability, which can be seen in Fig.5(b). All of the samples demonstrated excellent cycling stability, with minimal noticeable decreases after 100 cycles. This $LiFePO_4/LiCrTiO_4$ full cell retained 93.8% (115.6mAh·g^{-1}) of its initial specific discharge capacity after 100 cycles, demonstrating excellent cycling performance. The specific capacities of this material at 0.2, 0.5, 1C and 2C are 113, 110, 106 and 95mAh·g^{-1}[28-30], respectively. Except for the first cycle, the coulombic efficiency of the $LiFePO_4/LiCrTiO_4$ full cell was found to be over 99.5%, indicating excellent reversibility during electrochemical cycling.
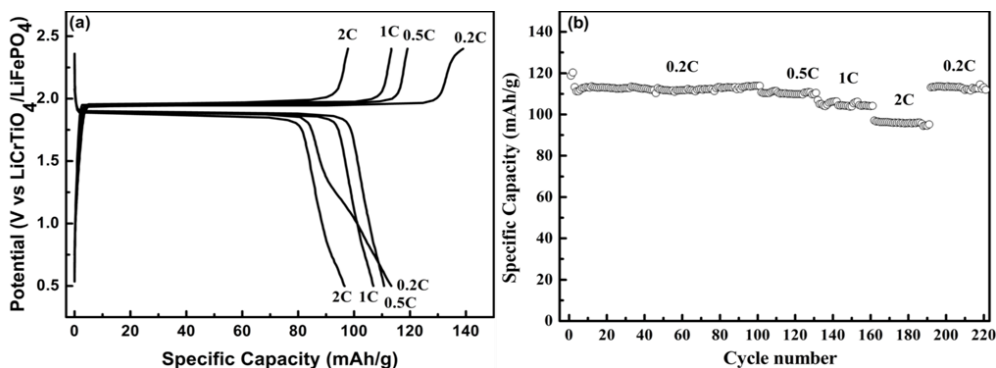
Figure 5. The charge and discharge curves(a) and cycling performance (b)of LiFePO$_4$/LiCrTiO$_4$ full cell at 0.2 ,0.5,1 and 2C in the voltage range of 0.5~2.4V.

The cyclic voltammograms (CVs) for the Li/LiCrTiO$_4$, Li/LiFePO$_4$ and LiFePO$_4$/LiCrTiO$_4$ are shown in Fig.6, all of which were performed at a scanning rate of 0.1mV·s^{-1}. The CV for the LiCrTiO$_4$ half-cell shows one anodic peak at ~1.58V and the corresponding cathodic peak at~1.47V. These peaks are attributed to the Ti$^{4+/3+}$[31-33]redox couple. The results confirm the reversible lithiation/delithiation behavior of LiCrTiO$_4$. The LiFePO$_4$/C electrodes show a pair of redox peaks at 3.51 V and 3.34V[10,11],consistent with the two-phase redox reaction of LiFePO$_4 \rightarrow$ FePO$_4$ + Li$^+$ + e$^-$. The LiFePO$_4$/LiCrTiO$_4$ full cell shows one anodic peak at~2.01V and the corresponding cathodic peak at~1.82V[28,30]. As shown in Fig.5, it is important to note that the separation of redox peaks is no more than 300mV at a scanning rate of 0.10mV·s^{-1} promising a high rate performance. After three cycles, well-overlapped peaks, better symmetry, and smaller potential interval values were visible, showing electrode reaction reversibility. The result indicates that the LiFePO$_4$/LiCrTiO$_4$ full cell may possess near perfect electrochemical behavior.
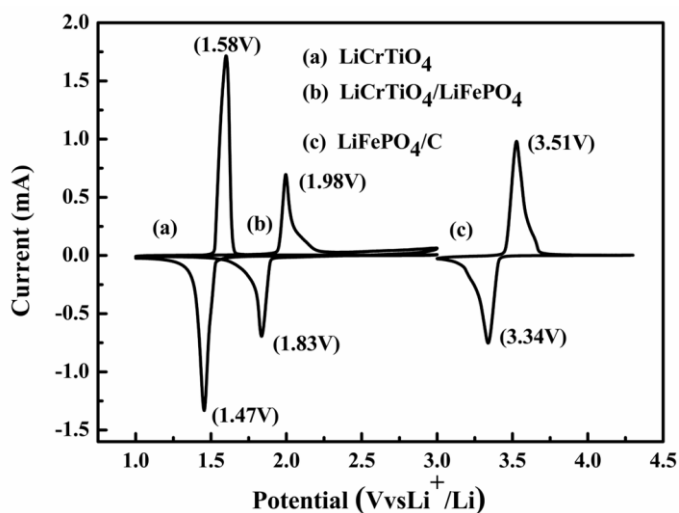

Figure 6. Cyclic voltammogram curves for Li/LiCrTiO$_4$, Li/LiFePO$_4$ half cell and LiFePO$_4$/LiCrTiO$_4$ full cells

EIS values for the materials were measured in a charged state after the first cycle to provide additional information on their electrochemical performance. The Nyquist plots and corresponding

circuits in Fig.7 all take the shape of a semicircle in the high-frequency region and a line in the low-frequency region. The reaction is controlled by both Warburg impedance for Li^+ diffusion, which is inversely proportional to the diffusion coefficient and the temporary, steady-state surface electrochemical reaction. Table1 shows the calculated electrochemical parameters for all samples. The $LiFePO_4/LiCrTiO_4$ full cell shows a much lower charge transfer resistance and warburg impedance than $LiFePO_4/C$. The conductivity values for $LiCrTiO_4$[7,8], $LiFePO_4/C$[18-20], and the $LiFePO_4/LiCrTiO_4$ full cell are on the order of 1.99×10^{-3}, 5.49×10^{-6} and $2.06\times10^{-3}S\cdot cm^{-1}$, respectively. This is due to the $LiCrTiO_4$ half-cell has a low charge transfer resistance and low warburg impedance. It also suggests that the $LiCrTiO_4$ material has good ionic conductivity.

Table 1. Fitting results of EIS data for as-prepared samples.

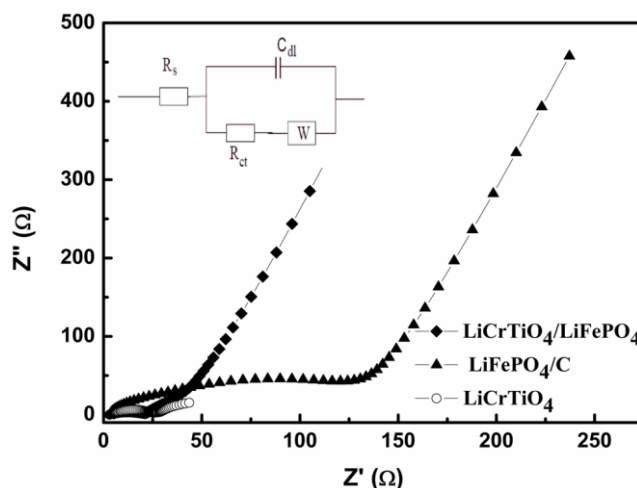| Cell	Rct (Ω)	W (Ω)	CPE (μF)
$Li/LiCrTiO_4$	34.95	70.24	1.99×10^{-3}
$Li/LiFePO_4$	178.73	141.13	5.49×10^{-6}
$LiFePO_4/LiCrTiO_4$	38.14	77.67	2.06×10^{-3}

Figure 7. AC impedance curves for $LiCrTiO_4$ half cell,$LiFePO_4/C$ half cell and $LiFePO_4/LiCrTiO_4$ full cell

4. CONCLUSIONS

Spinel structure $LiCrTiO_4$ was successfully synthesized via solid-state reaction, Electrochemical tests showed that $LiCrTiO_4$ has an excellent electrochemical capacity of $164.6mAh\cdot g^{-1}$ at 0.5C and $116.4mAh\cdot g^{-1}$ at 10C with stable cycling performance. This excellent cycle life and stability, as well as the fast and efficient synthetic method, make this process potentially feasible commercially. $LiFePO_4/LiCrTiO_4$ full cells exhibit a charge capacity of $136.6mAh\cdot g^{-1}$ and discharge

capacity of 116mAh·g^{-1} at 0.2C, and 96.4mAh·g^{-1} at 2C. LiFePO$_4$/LiCrTiO$_4$ full cells have a good cycling capacity and coulombic efficiency.

References

1. P. Lian, X. Zhu, S. Liang, Z. Li and H. Wang, *Electrochimica Acta*,55(2010)3909.
2. X. Yu, H. Pan, W. Wan, C. Ma, J. Bai, Q. Meng, Y. Hu and X. Yang, *Nano Lett.*, 13(2013) 4721.
3. A. Laumann, H. Boysen, M. Bremholm, K. Fehr, M. Hoelzel and M. Holzapfel, *Chem. Mater.*, 23(2011), 2753.
4. Y. Cheah, V. Aravindan and S. Madhavi, *ACS Appl. Mater. Interfaces*,5(2013)3475.
5. S. Hao, Xiao, Z. Hu, L. Sun, S. Han, D. Chen and X. Liu, *J.Am.Chem.Soc.,* 117(2013)26889.
6. Y. Wang, L. Gu, Y. Guo, H. Li, X. He, S. Tsukimoto, Y. Ikuhara and L. Wan, *J.Am.Chem.Soc.,* 134(2012)7874.
7. V. Aravindan, W. Chuiling and S. Madhavi, *J. Mater. Chem.,* 22(2012) 16026.
8. A. Kuhn, M. Martin and F. Garc$\acute{i}$a-Alvarado, *Z. Anorg. Allg. Chem.,*634(2008) 880.
9. R. Tan, R. Gao, Y. Zhao, M. Zhang, J. Xu, J. Ynag and P. Feng, *ACS Applied Materials & Interfaces*, 8(2016): 31273.
10. Y. Zhu, Y. Xu, Y. Liu, C. Luo and C.Wang, *Nanoscale*,5(2013)780.
11. Sun C., S. Rajasekhara, J. Goodenough and F. Zhou, *J.Am.Chem.Soc.,* 133(2011)2132.
12. L. Shen, H. Li, E. Uchaker, X. Zhang and G. Cao, *Nano Lett.*,12(2012) 5673.
13. J. Han, Y. Huang and J. Goodenough, *Chem. Mater.*, 23(2011)2027.
14. Y. Ma, B. Ding, G. Ji and J. Lee, *ACS nano.*,7(2013)10870.
15. T. Yuan, R. Cai and Z. Shao, *J. Phys. Chem. C.*,115(2011)4943.
16. Y. Zhang, C. Sun and Z. Zhou, *Electrochemistry Communications*, 11(2009)1183.
17. X. Feng, C. Shen, N. Ding and C. Chen, *J. Mater. Chem.*,22(2012)20861.
18. L. Noerochim, A. Yurwendra, and D. Susanti, *Ionics*, 22(2016): 341.
19. Z. Hu, D. Yang, K. Yin, J. Liu, F. Li, W. Gao, Y. Qin and H. Liu, *Advanced Materials Research*, 669(2013)311
20. C. Rao, and B. Rambabu, *Solid State Ionics*,181(2010) 839.
21. K. Lee and S. Song, *ACS Appl. Mater. Interfaces*, 3(2011)3697.
22. L. Wang, Q. Xiao, L. Wu, G. Lei, and Z. Li, *Solid State Ionics*, 236(2013)43.
23. Z. Yang, J. Xia, L. Zhi, W. Zhang and B. Pei, *Ionics*, 20(2014)169.
24. C. Sun, S. Rajasekhara, J. Goodenough, and F. Zhou, *J. Am. Chem. Soc.*, 133(2011) 2132.
25. W. Cui, Y. He, Z. Tang, Q. Yang, Q. Xu, Y. Su and L. Ma, *Journal of Solid State Electrochemistry,* 16(2012)265.
26. C. Yang, H. Hu, S. Lin and W. Chien, *Journal of Power Sources*, 258(2014)424.
27. A. Jaiswala, C. R. Hornea, O. Changa, W. Zhanga, W. Konga, E. Wangb, T. Chernb and M. Doeffb, *J. Electrochem. Soc.,*156(2009) 1041.
28. W. Wang, D. Choi and Z. Yang, *Metall and Mat Trans A.*, 44(2013): 21.
29. C. Yang, H. Hu, S. Lin and W. Chien, *Journal of Power Sources*, 258(2014): 424.
30. L. Xie, Y. Xu, J. Zhang, X. Cao, B. X.Yan and B.Qu *Int. J. Electrochem. Sci*, 8(2013): 1701.
31. X. Feng, H. Zou, H. Xiang, X. Guo, T. Zhou, Y. Wu, W. Xu, P. Yan, C. Wang, J. Zhang and Y. Yu, *ACS applied materials & interfaces*, 8(2016): 16718.
32. T. Zeng, X. Hu, P. Ji, Q.Peng and B.Shang *Int. J. Electrochem. Sci.*, 11(2016): 10199.

33. X. Li, Y. Huang, Y. Li, S. Sun, Y. Liu, J. Luo, J. Han and Y. Huang *RSC Adv.*, 7(2017): 4791.